Natural Resources for Human Health
eISSN: 2583-1194

Original Research

Received 15 July 2026
Revised 08 Aug 2026
Accepted 23 Aug 2026

Natural Resources for Human Health 2026, Vol. 6 (18s): 766–773

KEYWORDS:
Benzo[g]pterin; Pyrimidine derivatives; Ultrasound-assisted synthesis; Human thymidylate synthase (hTS); Molecular docking; Antitumor agents; Heterocyclic chemistry

Ultrasound-Assisted Synthesis, Spectroscopic Characterization, and Molecular Docking of Novel Benzo[g]pterin-Based Pyrimidine Derivatives against Human Thymidylate Synthase

Karm A. Khalaf[1] and Adnan O. Omar[2]
[1,2]Department of Chemistry, College of Science, University of Mosul, Mosul, Iraq.
*Correspondence; karm.21scp47@student.uomosul.edu.iq

ABSTRACT: A novel series of nitrogen-rich heterocyclic derivatives incorporating a fused benzo[g]pterin scaffold expanded with functionalized pyrimidine, pyrimidinone, pyrimidinethione, aminopyrimidine, and cyano-substituted motifs was designed and efficiently synthesized via ultrasound-assisted convergent routes. Using 2-aminobenzo[g]pteridin-4-one as a key synthon, three distinct synthetic pathways were established using activated methylene reagents (malononitrile or ethyl cyanoacetate), aromatic aldehydes, and various binucleophiles under acoustic cavitation. The target products (H1-H5 and K1–K6) were obtained in good to excellent isolated yields (60%–85%). Their chemical structures were unambiguously confirmed by FTIR, 1H-NMR, and 13C-NMR spectroscopic techniques. To evaluate their potential as targeted antitumor agents, representative derivatives spanning the synthetic series were subjected to molecular docking against human thymidylate synthase (hTS, PDB ID: 6QXG) and compared with the standard clinical antimetabolite 5-fluorouracil (5-FU). Among the evaluated compounds, derivative H1 exhibited an outstanding binding affinity (ΔG = -8.2 kcal/mol), significantly outperforming 5-FU (ΔG = -4.3 kcal/mol), H5 (ΔG = -4.4 kcal/mol), and K4 (ΔG = -3.8 kcal/mol). Detailed protein–ligand interaction profiling revealed that H1 accommodated precisely within the canonical catalytic pocket of hTS, forming key non-covalent interactions with crucial catalytic and binding-site residues, including Cys195, Asp218, Tyr258, Arg50, Arg215, Ser216, His256, and the intersubunit basic catalytic clamp Arg175/Arg176. These findings highlight the efficiency of the ultrasound-promoted synthetic protocols and position compound H1 as a highly promising hit structure for further biochemical and targeted anticancer evaluation.

1. INTRODUCTION

Pteridines are bicyclic nitrogen-containing heteroaromatic systems composed of fused pyrazine and pyrimidine rings. Their chemical and biological relevance has stimulated extensive medicinal-chemistry research, including antitumor, anti-inflammatory, antimicrobial, and other pharmacological applications. The pteridine framework also occurs in clinically important molecules and provides a versatile platform for the construction of hydrogen-bond-rich, electronically tunable heterocycles [1]. Benzo[g]pterin derivatives, including alloxazine-related systems, have likewise attracted interest because annulation with a benzene ring extends conjugation and provides additional opportunities for substitution and molecular recognition [2]. Pyrimidines constitute another privileged heterocyclic class. Their incorporation into fused and linked polyaza systems can substantially alter polarity, hydrogen-bonding capacity, tautomerism, and electronic distribution. Consequently, synthetic methods that efficiently assemble pyrimidine rings remain important in heterocyclic and medicinal chemistry. Ultrasound irradiation has increasingly been employed for pyrimidine synthesis and derivatization. Acoustic cavitation can

intensify mixing and mass transfer and, in suitable reaction systems, reduce reaction time or improve isolated yield relative to conventional procedures [3]. Malononitrile is particularly useful in multicomponent and cascade heterocyclic synthesis because its activated methylene group readily undergoes Knoevenagel condensation followed by nucleophilic addition and cyclization [4]. Human thymidylate synthase (hTS; EC 2.1.1.45) catalyzes the reductive methylation of dUMP to dTMP and is a validated anticancer target [5]. The clinical antimetabolite 5-fluorouracil requires intracellular metabolic activation, and its 5-fluoro-2'-deoxyuridine monophosphate (FdUMP) metabolite is the species that directly inhibits TS by forming a stable inhibitory complex with the enzyme and reduced-folate cofactor [6, 7].

The FdUMP-bound human TS crystal structure 6QXG was solved by X-ray diffraction at 2.08 Å resolution and provides a structurally defined catalytic cavity for ligand-docking studies [8]. These features motivated a structure-based assessment of representative members of the newly synthesized H- and K-series. In the present work, a series of novel benzo[g]pterin-based derivatives was prepared through three complementary synthetic approaches. The first uses malononitrile and substituted aromatic aldehydes to construct cyano/amino heterocyclic products. The second proceeds through an α, β-unsaturated amide followed by cyclocondensation to afford pyrimidinone, pyrimidinethione, and amino-pyrimidine analogues. The third employs ethyl cyanoacetate, aromatic aldehydes, and X-substituted amidine-type reagents to generate six K-series products. The structures were evaluated using FTIR, 1H-NMR, and 13C-NMR spectroscopy together with physical properties and isolated yields. In addition, representative derivatives H1, H5, and K4 were subjected to molecular docking against hTS (PDB 6QXG) and compared with 5-FU to examine whether the synthesized scaffolds can access functionally relevant regions of the TS binding cavity.

2. MATERIALS AND METHODS

2.1 Materials and instrumentation

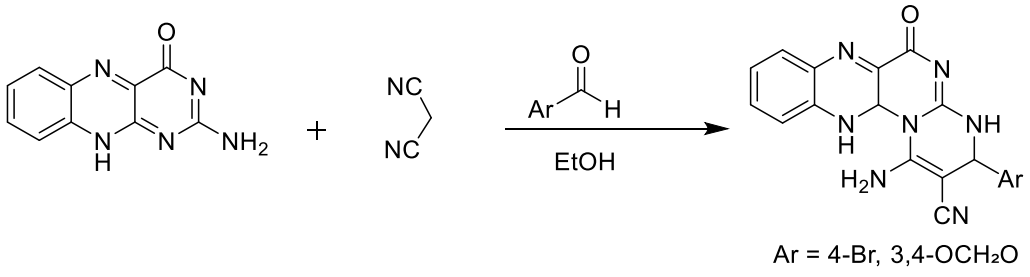
Some of the chemicals and solvents were available in the Department of Chemistry at the University of Mosul, while the remaining reagents were purchased from commercial suppliers and used without further purification. Ethanol was employed as the reaction solvent [9]. Melting points of the synthesized compounds were measured in open capillary tubes and are reported uncorrected. FTIR spectra were recorded using KBr pellets on a Bruker FTIR spectrometer and are reported as υ (cm-1). 1H-NMR (400 MHz) and 13C-NMR (100.6 MHz) spectra were recorded on a Bruker AVANCE NEO 400 MHz spectrometer using DMSOd6 as the solvent, with chemical shifts (δ) given in ppm.

2.2 General ultrasound-assisted procedure

The appropriate reactants were combined in ethanol according to the synthetic sequence described below and exposed to ultrasonic irradiation until completion of the reaction. After completion, the reaction mixture was worked up and the resulting solid was isolated and purified to furnish the target derivative [10].

2.3. Synthetic route A: cyano-substituted benzo[g] pterin derivatives (H1, H2).

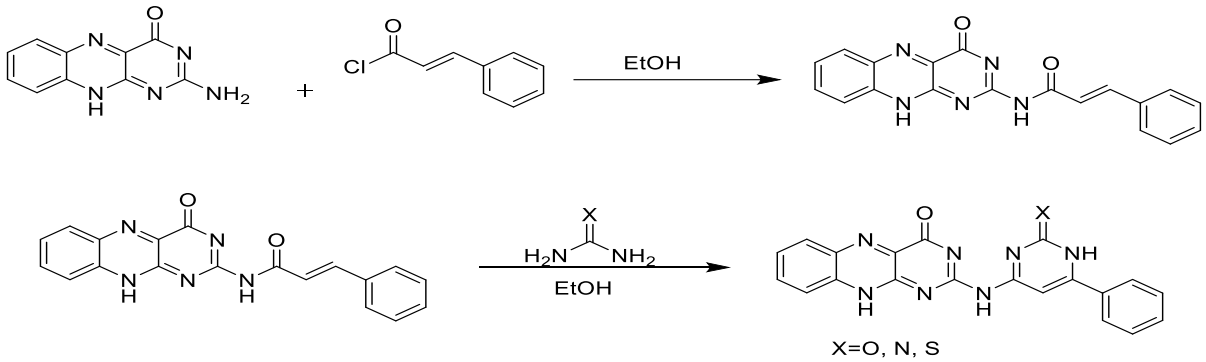
The synthesis of compounds was achieved by reacting 2-amino-benzo[g]pteridin-4-one, malononitrile, and aromatic aldehydes (Ar–CHO) in ethanol, following Knoevenagel condensation and intramolecular cyclization (Scheme 1). The resulting p-bromophenyl and benzodioxolyl derivatives were purified by recrystallization from ethanol. Melting points were recorded [11]. FTIR spectra (KBr) were recorded on a Bruker FTIR spectrometer. 1H-NMR (400 MHz) and 13C-NMR (100.6 MHz) spectra were obtained on a Bruker AVANCE NEO 400 MHz spectrometer in DMSO-d6 (δ, ppm).



Natural Resources for Human Health
eISSN: 2583-1194

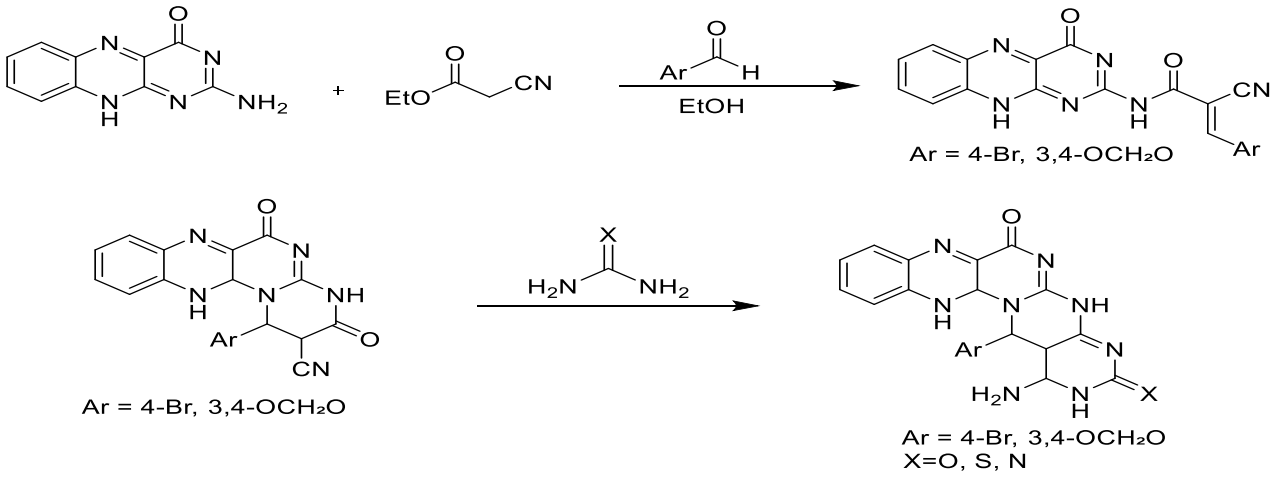
2.4 Synthetic route B: pyrimidinone, pyrimidinethione and amino-pyrimidine derivatives (H3, H4, H5)

The amino-benzo[g]pterin precursor was first acylated with an α,β-unsaturated acyl chloride (cinnamoyl-type reagent) to generate an α,β-unsaturated amide intermediate. Subsequent reaction with H2N–C(=X)–NH2 type cyclizing reagents produced the corresponding oxygen, sulfur, and amino ،containing pyrimidine derivatives via conjugate addition/cyclocondensation and ring closure (Scheme 2). All synthesized products were purified by recrystallization from ethanol [12].



2.5. Synthetic route C: K1–K6 derivatives

The amino-benzo[g]pterin precursor was converted to a cyanoacetamide type intermediate using ethyl cyanoacetate. Condensation with an aromatic aldehyde generated an α, β-unsaturated cyanoamide intermediate. Treatment with urea-, thiourea-, or guanidine-type reagents afforded three cyclized products for each aromatic substituent [13]. Two aromatic series were used a bromophenyl series (K1–K3) and a benzodioxole series (K4–K6), providing six final derivatives (Scheme 3). All synthesized products were purified by recrystallization from ethanol.



2.6. Molecular docking protocol

The X-ray crystal structure of human thymidylate synthase in complex with FdUMP (PDB ID: 6QXG; 2.08 Å resolution) was used as the receptor template [14]. Solvent molecules and the co-crystallized ligand were removed during receptor preparation, while the experimentally defined FdUMP cavity was used as the structural reference for the catalytic binding region [15]. The synthesized ligands were prepared in three-dimensional form and docked using the same scoring workflow applied to the reference compound [16]. The best-ranked poses were subsequently inspected by two-dimensional protein-ligand interaction mapping. Reported docking scores are expressed in kcal/mol; more negative values indicate more favorable scores within the employed scoring function. Because 5-FU is metabolically converted to FdUMP before direct inhibition of TS, 5-FU was retained as a clinically relevant drug comparator, whereas the FdUMP-bound 6QXG structure served as the mechanistic structural reference [17]. For cross-series comparison with the currently available docking dataset, H1, H5, and K4 were selected

as representative products from Routes A, B, and C, respectively. The docking outputs were interpreted conservatively because docking scores are model-dependent and do not constitute experimental inhibition constants [18].

3. RESULTS AND DISCUSSION

3.1. Chemistry and reaction rationale

The synthetic design exploits the nucleophilicity of the exocyclic amino group of the benzo[g]pterin precursor and the high reactivity of activated methylene compounds [19]. Malononitrile and cyanoacetate-derived intermediates facilitate carbon–carbon bond formation with aromatic aldehydes through Knoevenagel-type condensation [20]. The resulting electron-deficient alkenes are suitable substrates for subsequent nucleophilic addition and intramolecular cyclization. In the K-series, changing the cyclizing reagent alters the heteroatom functionality of the newly formed pyrimidine ring, whereas changing Ar from p-bromophenyl to benzodioxole modulates the peripheral aromatic substituent.

3.2 Physical properties and isolated yields

The reported yields range from 60 to 85%. H1 showed the highest yield (85%), followed by K3 (84%) and K2 (80%). Within the K-series, melting points ranged from 130 °C for K2 to 232 °C for K6. The higher melting points of K5 and K6 may reflect differences in crystal packing, intermolecular hydrogen bonding, polarity, and molecular rigidity; however, melting-point differences alone cannot establish a specific intermolecular mechanism without solid-state data.

Table 1. Physical properties, isolated yields, molecular weights, and molecular formulas of the synthesized H- and K-series derivatives.

Compound	M.P. (°C)	Yield (%)	Color	Molecular weight	Molecular formula
H1	138	85	Brown	446.27	C20H12BrN7O
H2	202	75	Brown	411.38	C21H13N7O3
H3	148	65	Cream	383.37	C20H13N7O2
H4	138	60	Yellow	384.4	C20H16N8O
H5	154	60	Orange	399.09	C20H13N7OS
K1	167	60	Red	493.33	C21H17BrN8O2
K2	130	80	Yellow	509.39	C21H17BrN8OS
K3	155	84	Yellow	492.34	C21H18BrN9O
K4	184	60	Brown	458.44	C22H18N8O4
K5	212	65	Yellow	474.5	C22H18N8O3S
K6	232	60	Brown	457.45	C22H19N9O3

3.3 FTIR spectroscopic characterization

The FTIR data support the functional-group changes expected from the proposed transformations. The cyano-containing products showed sharp C≡N absorptions at 2218 and 2223 cm−1, providing direct evidence for retention of the nitrile functionality after cyclization. NH2 bands were reported near 3421–3438 cm−1 and NH absorptions near 3184–3204 cm−1 in these derivatives. Carbonyl absorptions were observed in the ca. 1700 cm−1 region, consistent with the benzo[g]pterin-4-one core and, where applicable, an additional pyrimidinone carbonyl. In sulfur-containing derivatives, C=S absorptions were observed at approximately 1220–1227 cm−1 in the K-series and at 1350 cm−1 in the H-series, which is consistent with the sensitivity of C=S stretching vibrations to conjugation and structural coupling.

3.4. 1H-NMR analysis

The 1H NMR spectra are consistent with the proposed nitrogen-rich heterocyclic products. Exchangeable NH resonances occur predominantly in the downfield region, commonly around δ 9–11.8 ppm, reflecting attachment to conjugated heteroaromatic and carbonyl-containing systems. Aromatic protons appear as multiplets mainly between δ 7 and 8.5 ppm. Exocyclic NH2 groups give broad or singlet resonances in the approximately δ 4–7 ppm region depending on the local electronic environment and hydrogen bonding. In benzodioxole-containing derivatives, the O–CH2–O group gives a characteristic signal around δ 5.9–6.4 ppm in the supplied data. The appearance of new methine/heterocyclic CH resonances and disappearance of precursor alkene or activated-methylene patterns support ring formation.

3.5. 13C-NMR analysis

The 13C NMR spectra further support the assigned structures. Carbonyl carbons of the benzo[g]pterin/pyrimidinone systems occur in the downfield region around δ 164–171 ppm in the supplied spectra. Thiocarbonyl derivatives exhibit markedly deshielded C=S resonances near δ 178.5–181.7 ppm, a useful diagnostic distinction from their oxygen analogues. Heterocyclic C=N/C–N carbons generally occur between approximately δ 148 and 161 ppm, while aromatic carbons occupy the expected δ 110–145 ppm region. Benzodioxole O–CH2–O carbons occur in the characteristic oxygenated aliphatic region, while newly generated saturated heterocyclic carbons appear further upfield.

3.6. Representative spectral assignments

For the p-bromophenyl cyano derivative, the supplied FTIR spectrum lists ν(C≡N) at 2218 cm−1, ν(NH2) at 3438 cm−1, and ν(NH) at 3204 cm−1. Its 1H NMR spectrum contains δ 9.99 (s, 1H, NH), 8.53–7.46 (m, aromatic H), 6.08 (s, 1H, CH), and 4.49 (br s, 2H, NH2). The 13C NMR spectrum includes δ 165.45 (C=O), 160.29, 150.52, and 148.88 (heterocyclic C=N/C–N), with additional aromatic/heterocyclic signals and a methine resonance at δ 57.53. The benzodioxole cyano analogue similarly shows ν(C≡N) at 2223 cm−1 and an OCH2O proton resonance at δ 6.224 ppm. These diagnostic features support the assigned products.

3.7. Effect of ultrasound and methodological limitation

Ultrasound is well established as a process-intensification tool in heterocyclic synthesis, particularly for pyrimidine-forming cyclocondensations and malononitrile-based multicomponent reactions [3,4]. Cavitation can improve local mixing and mass transfer and may accelerate reactions. Nevertheless, the present dataset, as supplied, does not include a conventional-heating control performed under otherwise comparable conditions. Therefore, the manuscript should describe the reactions as ultrasound-assisted but should not claim that ultrasound increased yield, shortened reaction time, or improved selectivity unless comparative experimental data are added.

3.8. Molecular docking against human thymidylate synthase

The docking results differentiated the representative derivatives both by absolute score and by binding-site location [21]. H1 produced the most favorable docking score (ΔG= -8.2 kcal/mol), compared with -4.3 kcal/mol for 5-FU, (ΔG= -4.4 kcal/mol) for H5, and (ΔG= -3.8 kcal/mol) for K4 (Table 2). H1 was positioned within the canonical hTS catalytic cavity and contacted residues associated with nucleotide recognition and catalysis, including Cys195, Asp218, Tyr258, Arg50, Arg215, Ser216, His256, Arg175, and Arg176.

The catalytic Cys195 is positioned in native hTS to attack the uracil C6 atom, whereas Arg50, Arg215, Arg175', and Arg176' contribute to nucleotide-phosphate recognition in the dUMP/FdUMP complex [7]. The H1 pose therefore provides a structurally plausible basis for prioritizing this derivative for enzyme-level testing. K4 occupied the same general catalytic region and contacted Cys195, Arg50, Arg215, Asp218, Tyr258, Arg175, and Arg176. However, the interaction map also contained unfavorable donor-donor and/or positive-positive contacts involving basic residues, providing a plausible qualitative explanation for its less favorable score.

In contrast, H5 was predicted at a peripheral site dominated by Gln32, Gln62, Arg64, Ala63, Ser66, Leu31, and nearby residues rather than the canonical catalytic pocket. The 5-FU pose generated in the current workflow similarly involved residues around

Gln160, Arg163, Val164, Asp174, Ile177, and Ile178 and did not reproduce the FdUMP-site interaction network. Accordingly, the H5 and 5-FU scores are reported descriptively but are not treated as direct active-site affinity comparators to H1 and K4.

Table 2. Predicted docking scores, score-normalized ligand-efficiency estimates, key contacts, and pose interpretation for 5-FU and representative H/K derivatives against hTS (6QXG).

Ligand	Docking score (kcal/mol)	Score-normalized LE	Key contacts observed	Pose interpretation
5-FU	-4.3	0.48	Gln160, Arg163, Val164, Asp174, Ile177, Ile178	Noncanonical pose in current workflow
H1	-8.2	0.28	Cys195, Asp218, Tyr258, Arg50, Arg215, Ser216, His256, Arg175/176	Canonical catalytic cavity; best absolute score
H5	-4.4	0.15	Gln32, Gln62, Arg64, Ala63, Ser66, Leu31	Peripheral/noncanonical pose
K4	-3.8	0.11	Cys195, Arg50, Arg215, Asp218, Tyr258, Arg175/176	Catalytic cavity; unfavorable contacts present

Absolute docking scores may favor larger ligands because they can form more contacts. As a size-normalized descriptive check, the magnitude of the docking score divided by the number of heavy atoms gives approximate score-normalized ligand-efficiency values of 0.48 for 5-FU, 0.28 for H1, 0.15 for H5, and 0.11 kcal mol-1 per heavy atom for K4. This normalization reinforces the need to avoid interpreting the more negative H1 score as direct evidence of superior pharmacological potency [22]. Instead, the key outcome is that H1 combines the most favorable absolute score among the tested derivatives with a pose that engages the recognized catalytic cavity.

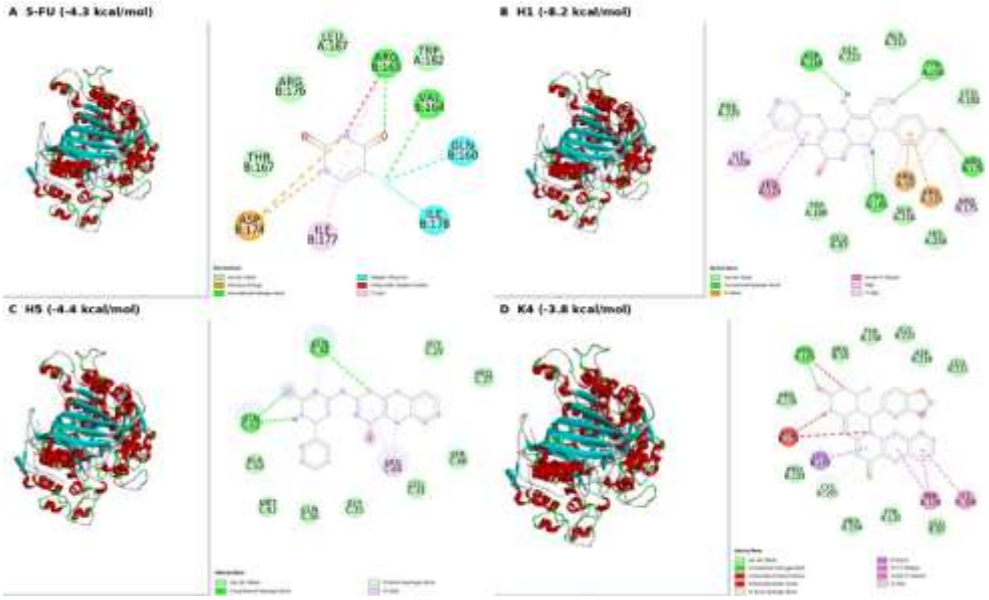


Figure 1. Representative docking interaction maps for (A) 5-FU, (B) H1, (C) H5, and (D) K4 against human thymidylate synthase (6QXG). H1 and K4 occupy the catalytic region, whereas the current H5 and 5-FU poses are noncanonical relative to the FdUMP-binding cavity.

4. PROPOSED MECHANISTIC PATHWAYS

Route A is proposed to begin with Knoevenagel condensation between Ar–CHO and malononitrile, producing Ar–CH=C(CN)2. Nucleophilic attack by the exocyclic amino group of the benzo[g]pterin precursor, followed by intramolecular attack on a nitrile group, proton transfers, and aromatization, generates the amino-cyano annulated product.

In Route B, nucleophilic acyl substitution of the amino-benzo[g]pterin precursor on the α, β-unsaturated acyl chloride affords an unsaturated amide. Addition of the bifunctional N-nucleophile, followed by intramolecular cyclocondensation and dehydration/tautomerization, gives the corresponding pyrimidinone, pyrimidinethione, or amino-pyrimidine derivative.

In Route C, reaction with ethyl cyanoacetate forms a cyanoacetamide intermediate. Knoevenagel condensation with Ar–CHO then generates an arylidene cyanoamide. Addition of urea, thiourea, or the corresponding guanidine-type reagent across the activated system, followed by ring closure and proton rearrangement, furnishes K1–K6.

5. CONCLUSION

A structurally diverse series of benzo[g]pterin-based pyrimidine derivatives was obtained through modular annulation and cyclocondensation strategies. The reported isolated yields were moderate to high (60-85%), and FTIR, 1H NMR, and 13C NMR data supported formation of the proposed nitrogen-rich heterocyclic frameworks. Structure-based docking against human thymidylate synthase extended the experimental study by examining representative derivatives from the three synthetic routes. H1 produced the most favorable absolute score (-8.2 kcal/mol) and, importantly, occupied the recognized catalytic cavity with contacts involving Cys195, Asp218, Tyr258, Arg50, Arg215, Ser216, His256, and the intersubunit Arg175/Arg176 region. K4 also accessed the catalytic cavity but displayed unfavorable contacts, whereas H5 and the 5-FU pose generated by the current workflow were noncanonical relative to the FdUMP site. The docking data therefore support H1 as the principal candidate for subsequent hTS enzyme-inhibition and anticancer evaluation, but they do not establish biological potency on their own. Future work should include biochemical TS inhibition measurements, broader docking of the remaining H- and K-series, redocking of the crystallographic FdUMP ligand for protocol validation, and orthogonal structural/purity confirmation such as HRMS and/or elemental analysis.

REFERENCES

[1] Carmona-Martínez V, Ruiz-Alcaraz AJ, Vera M, Guirado A, Martínez-Esparza M, García-Peñarrubia P. Therapeutic potential of pteridine derivatives: A comprehensive review. Medicinal Research Reviews. 2019;39(2):461-516. doi:10.1002/med.21529.

[2] Samaha D, Mahmoud S, Mohamed MS, Abdullah RS, Abou Taleb NA, Nagamatsu T, Ali HI. Novel alloxazine analogues: design, synthesis, and antitumour efficacy enhanced by kinase screening, molecular docking, and ADME studies. Journal of Enzyme Inhibition and Medicinal Chemistry. 2024;39(1):2398551. doi:10.1080/14756366.2024.2398551.

[3] Mittersteiner M, Farias FFS, Bonacorso HG, Martins MAP, Zanatta N. Ultrasound-assisted synthesis of pyrimidines and their fused derivatives: A review. Ultrasonics Sonochemistry. 2021;79:105683. doi:10.1016/j.ultsonch.2021.105683.

[4] Javahershenas R, Nikzat S. Recent developments using malononitrile in ultrasound-assisted multicomponent synthesis of heterocycles. Ultrasonics Sonochemistry. 2024;102:106741. doi:10.1016/j.ultsonch.2023.106741.

[5] Dofe VS, Sarkate AP, Shaikh ZM, Jadhav CK, Nipte AS, Gill CH. Ultrasound-assisted synthesis of novel pyrazole and pyrimidine derivatives as antimicrobial agents. Journal of Heterocyclic Chemistry. 2018;55(3):756-762. doi:10.1002/jhet.3105.

[6] Parker WB, Cheng YC. Metabolism and mechanism of action of 5-fluorouracil. Pharmacology & Therapeutics. 1990;48(3):381-395. doi:10.1016/0163-7258(90)90056-8.

[7] Peters GJ, Backus HHJ, Freemantle S, et al. Induction of thymidylate synthase as a 5-fluorouracil resistance mechanism. Biochimica et Biophysica Acta - Molecular Basis of Disease. 2002;1587(2-3):194-205. doi:10.1016/S0925-4439(02)00082-0.

[8] Pozzi C, Ferrari S, Luciani R, Tassone G, Costi MP, Mangani S. Structural comparison of Enterococcus faecalis and human thymidylate synthase complexes with the substrate dUMP and its analogue FdUMP provides hints about enzyme conformational variabilities. Molecules. 2019;24(7):1257. doi:10.3390/molecules24071257.

[9] Pavia, D. L., Lampman, G. M., Kriz, G. S., & Vyvyan, J. R. (2014). Introduction to spectroscopy (5th ed.). Cengage Learning.

[10] Mason, T. J. (2007). Sonochemistry and the environment—Providing a green link. Green Chemistry, 9(1), 49–53. https://doi.org/10.1039/B612261M

[11] El-Khateeb, A. Y., Hamed, S. E., & Elattar, K. M. (2022). Recent advancements in the multicomponent synthesis of heterocycles integrated with a pyrano[2,3-d]pyrimidine core. RSC Advances, 12(19), 11808–11842. https://doi.org/10.1039/d2ra00927g

[12] Maddila, S., Gorle, S., Sreekanth, B., & Jonnalagadda, S. B. (2016). Synthesis and biological evaluation of new pyrimidinone and pyrimidinethione derivatives via cyclocondensation. Journal of Heterocyclic Chemistry, 53(5), 1540–1546. https://doi.org/10.1002/jhet.2461

[13] Fadda, A. A., Abdel-Latif, E., & El-Defrawy, A. M. (2012). Synthetic utility of ethyl cyanoacetate in heterocyclic synthesis. Journal of Heterocyclic Chemistry, 49(2), 223–242. https://doi.org/10.1002/jhet.819

[14] Pozzi, C., Lopresti, L., Luciani, R., Santucci, M., Costi, M. P., & Mangani, S. (2019). Crystal structure of human thymidylate synthase in complex with FdUMP. Protein Data Bank (PDB). https://doi.org/10.2210/pdb6QXG/pdb

[15] Longley, D. B., Harkin, D. P., & Johnston, P. G. (2003). 5-Fluorouracil: Mechanisms of action and clinical strategies. Nature Reviews Cancer, 3(5), 330–338. https://doi.org/10.1038/nrc1074

[16] Santi, D. V., McHenry, C. S., & Sommer, H. (1974). Mechanism of interaction of thymidylate synthetase with 5-fluorodeoxyuridylate. Biochemistry, 13(3), 471–481. https://doi.org/10.1021/bi00700a012

[17] Meng, X. Y., Zhang, H. X., Mezei, M., & Cui, M. (2011). Molecular docking: A powerful approach for structure-based drug discovery. Current Computer-Aided Drug Design, 7(2), 146–157. https://doi.org/10.2174/157340911795677602

[18] Kitchen, D. B., Decornez, H., Furr, J. R., & Bajorath, J. (2004). Docking and scoring in virtual screening for drug discovery: Methods and applications. Nature Reviews Drug Discovery, 3(11), 935–949. https://doi.org/10.1038/nrd1549

[19] Jadhav, A. L., & Yadav, G. D. (2019). Clean synthesis of benzylidenemalononitrile by Knoevenagel condensation of benzaldehyde and malononitrile: Effect of combustion fuel on activity and selectivity of Ti-hydrotalcite and Zn-hydrotalcite catalysts. Journal of Chemical Sciences, 131(8), Article 79. https://doi.org/10.1007/s12039-019-1641-6

[20] Yamazaki, S., Katayama, K., Wang, Z., Mikata, Y., Morimoto, T., & Ogawa, A. (2021). Sequential Knoevenagel condensation/cyclization for the synthesis of indene and benzofulvene derivatives. ACS Omega, 6(42), 28441–28454. https://doi.org/10.1021/acsomega.1c05283

[21] Phan, J., Koli, S., Minor, W., Dunlap, R. B., Berger, S. H., & Lebioda, L. (2001). Structural basis for the catalysis and inhibition of human thymidylate synthase. Protein Science, 10(8), 1571–1580. https://doi.org/10.1110/ps.07001

[22] Hopkins, A. L., Groom, C. R., & Alex, A. (2004). Ligand efficiency: A useful metric for lead selection. Drug Discovery Today, 9(10), 430–431. https://doi.org/10.1016/S1359-6446(04)03069-7